Submitted to Engineering Fracture Mechanics

IMPROVED QUARTER-POINT CRACK TIP ELEMENT

L. J. Gray[1] A.-V. Phan[1], Glaucio H. Paulino[2] and T. Kaplan[1]

August 11, 2001

[1]Computer Science and Mathematics Division, Oak Ridge National Laboratory, Oak Ridge, Tennessee 37831-6367

[2]Department of Civil and Environmental Engineering, University of Illinois, Urbana-Champaign, IL 61801-2352

Abstract

We present a modification to the quarter-point crack tip element and employ this element in two-dimensional boundary integral fracture analysis. The standard singular element is adjusted so that the near-tip crack opening displacement satisfies a known constraint: the coefficient of the term which is linear in the distance to the tip must vanish. Stress intensity factors calculated with the Displacement Correlation Technique are shown to be highly accurate, and significantly more accurate than with the standard element. The improvements are especially dramatic for mixed-mode problems involving curved and interacting cracks.

Key words. Fracture mechanics, stress intensity factors, quarter-point element, boundary integral analysis

Abbreviated title: Improved Quarter-Point

1 Introduction

The numerical modeling of crack stability and propagation (Rice 1968) requires the accurate determination of stress intensity factors (SIFs), which in turn relies on the correct representation of the local crack tip stress and displacement fields. For a crack geometry, William's (1952, 1957) result for the displacement $\mathbf{u} = u_k,\ k = 1, 2$, in the neighborhood of the tip is:

$$u_k(r, \theta) = a_k + b_k(\theta) r^{\frac{1}{2}} + c_k(\theta) r + d_k(\theta) r^{\frac{3}{2}} + \dots \ , \tag{1}$$

where $r,\ \theta$ are the distance to, and the direction emanating from, the tip, respectively. Thus the crack opening displacement $\Delta\mathbf{u} = \Delta u_k,\ k = 1, 2$ at the tip, is

$$\Delta u_k(r, \theta) = b_k(\theta) r^{\frac{1}{2}} + c_k(\theta) r + d_k(\theta) r^{\frac{3}{2}} + \dots \quad . \tag{2}$$

In both finite and boundary element modeling of discrete cracks, the standard approach consists of incorporating the critical $\sqrt{r}$ behavior by means of the 'quarter-point' element originally developed by Henshell and Shaw (1975), and Barsoum (1976). Use of special elements at the crack tip has significantly improved the accuracy of stress intensity factor (SIF) calculations (Blandford *et al.* 1981; Sladek and Sladek 1986; Linkov and Mogilevskaya 1994) , and the original quarter-point element has been extended and refined in a number of ways (Banks-Sills 1991; Lim *et al.* 1993; Horváth 1994). Nevertheless, in either finite or boundary element analyses, the prediction of sliding and twisting stress intensity modes, $K_{II},\ K_{III}$, has not been nearly as accurate as for the opening mode K_I.

Recently, Gray and Paulino (1998) proved that, irrespective of the problem geometry or boundary conditions, the series expansion in Eq. (2) must have $c_k = 0$ for $\Delta\mathbf{u}$ *on the crack surface* (for related work see Martin 1991). As will be discussed below, in general the quarter-point element fails to satisfy this constraint, and it is this flaw that is addressed in this paper. By forcing the linear term in $\Delta\boldsymbol{u}$ to be zero, we expect to have a more accurate analysis in the tip region. This is in fact borne out by the test calculations, as a dramatic improvement in the accuracy of stress intensity factors is seen. These calculations employ a Symmetric-Galerkin boundary integral fracture analysis (see, for example, Sirtori *et al.* 1992 and Bonnet *et al.* 1998) coupled with a Displacement Correlation technique for evaluating the SIFs.

The remaining sections of this paper are organized as follows. The next section presents the shape functions for the improved quarter-point element. The symmetric-Galerkin boundary integral approximation for modeling generic fracture mechanics problems, to be used in the computational examples, is reviewed in Section 3. The numerical examples in Section 4 treat several different crack configuations, and display the superiority of the modified quarter-point element over the standard element. Finally, some closing remarks are given.

2 Modified Quarter-Point Element

The two-dimensional quarter-point element is based upon the three-noded quadratic element. For $t \in [0,\ 1]$, the shape functions for this element are given by

$$\begin{aligned} \psi_1(t) &= (1-t)(1-2t)\ , \\ \psi_2(t) &= 4t(1-t)\ , \\ \psi_3(t) &= t(2t-1)\ . \end{aligned} \tag{3}$$

As $\Delta u = 0$ at the crack tip, assumed to be at $t = 0$, the representations of the crack tip geometry and crack opening displacement are

$$\begin{aligned} \Gamma(t) &= \sum_{j=1}^{3} (x_j \psi_j(t),\ y_j \psi_j(t)) \\ \Delta u_k(t) &= \sum_{j=2}^{3} \left(\Delta u_1^j \psi_j(t),\ \Delta u_2^j \psi_j(t)\right)\ . \end{aligned} \tag{4}$$

Here (x_j, y_j) are the coordinates of the three nodes defining the element, and Δu_k^j the nodal values of the crack opening displacement (COD).

Henshell and Shaw (1975) and independently Barsoum (1976), demonstrated that by moving the mid-node coordinates (x_2, y_2) three fourths of the way towards the tip, the parameter t becomes $\sqrt{r/L}$, with L being the distance from (x_1, y_1) to (x_3, y_3). As a consequence, the leading order term in Δu_k^j at $t = 0$, which is t, is the correct square root of distance . Note however, that the next term, which is t^2, is r/L. According to Gray and Paulino (1998), this term should vanish, and the modification presented below replaces this term with $(r/L)^{3/2}$.

For the new approximation, we keep the representation of $\Gamma(t)$ as in Eq. (4), so that the property $t \approx \sqrt{r}$ remains, and the interpolation of the geometry remains quadratic. However for the COD, we define new shape functions by adding a cubic term:

$$\begin{aligned} \hat{\psi}_2(t) &= 4t(1-t) - 4t(1-t)(1-2t)/3 = -\frac{8}{3}(t^3 - t)\ , \\ \hat{\psi}_3(t) &= t(2t-1) + 2t(1-t)(1-2t)/3 = \frac{4}{3}(4t^3 - t)\ . \end{aligned} \tag{5}$$

This additional contribution accomplishes the cancellation of the $t^2 \approx r$ term, without disturbing the interpolation, *i.e.*,

$$\hat{\psi}_2(0) = 0\ , \qquad \hat{\psi}_2(1/2) = 1\ , \qquad \hat{\psi}_2(1) = 0 \quad , \tag{6}$$

$$\hat{\psi}_3(0) = 0 \ , \qquad \hat{\psi}_3(1/2) = 0 \ , \qquad \hat{\psi}_3(1) = 1 \quad . \tag{7}$$

As might be expected, this alteration does not radically alter the COD shape functions, as seen in Fig. 1.

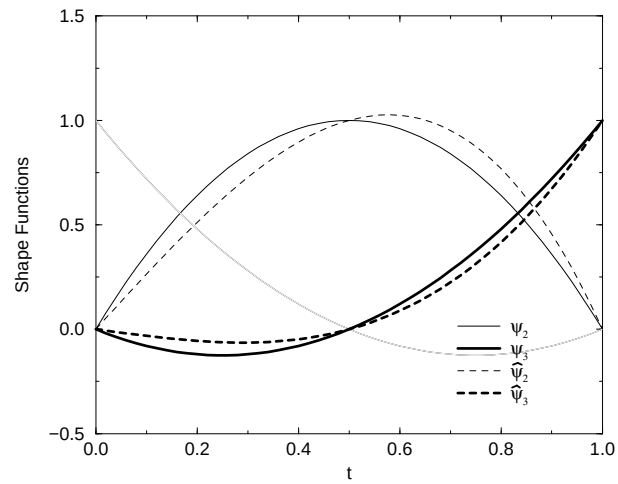

Figure 1: Standard $(Q2, Q3)$ and modified $(M2, M3)$ shape functions.

3 Symmetric Galerkin Boundary Integral Fracture Analysis

The test calculations reported below employ a two-dimensional Symmetric-Galerkin approximation, and thus this section presents a quick overview of this technique. A good introduction to the Galerkin method is provided in the recent text by Bonnet (1995), and a recent review by Bonnet *et al.* (1998) on Symmetric-Galerkin provides an excellent summary and references to the literature. The primary motivation for this brief review is to point out that, in the Galerkin approach, the shape functions do more than simply define the interpolation approximations for the surface and boundary functions: they are directly involved in how the continuous integral equations are reduced to finite matrices. Thus, in this approach, the change from the standard quater-point element to the new one will significantly impact the approximation.

The two-dimensional displacement boundary integral equation is given by (Rizzo 1967;

Cruse 1988)

$$\mathcal{U}(P) = u_k(P) + \int_{\partial B} T_{kj}(P,Q)u_j(Q)\,dQ - \int_{\partial B} U_{kj}(P,Q)\tau_j(Q)\,dQ = 0 \ , \qquad (8)$$

where $\mathbf{u}$ and $\boldsymbol{\tau}$ denote displacement and traction, respectively. As customary, the kernel functions $T_{kj}(P,Q)$ and $U_{kj}(P,Q)$ are given by the Kelvin solution for a point load in an infinite medium (formulas for these functions, along with those for the stress equation below, can be found in the Appendix). The corresponding integral equation for the surface stress is essential for treating crack geometries, and in the Symmetric-Galerkin approach it is this equation that is employed on the crack surface. The stress equation (from which one gets an equation for surface traction by multiplying by the appropriate normal vector) is obtained by differentiating Eq. (8) with respect to P, resulting in

$$\mathcal{S}(P) = \sigma_{lk}(P) + \int_{\partial B} S_{lkm}(P,Q)u_m(Q)\,dQ - \int_{\partial B} D_{lkm}(P,Q)\tau_m(Q)\,dQ = 0 \ . \qquad (9)$$

In a Galerkin formulation, the above integral equations are enforced 'on average', in the form

$$\begin{aligned} \int_{\partial B} \psi_l(P)\mathcal{U}(P)\,\mathrm{d}P &= 0 \ , \\ \int_{\partial B} \psi_l(P)\mathcal{S}(P)\,\mathrm{d}P &= 0 \ . \end{aligned} \qquad (10)$$

The weight functions $\psi_l(P)$ are the shape functions employed to interpolate the boundary displacements and tractions. Again, note that the modified shape functions for the quarter-point are employed to define the Galerkin equations in the crack tip region.

For symmetric-Galerkin (Sirtori 1979, Hartmann et al. 1985), the displacement equation is employed on the part of the boundary where displacement is specified, while the traction equation is employed on the part of the boundary where traction is known. As the name implies, this results in a symmetric coefficient matrix. This remains true for fracture problems, with the proviso that the unknowns on the crack surface are now the jump in displacement.

A key advantage of the Galerkin approach is that the extra boundary integration simplifies the task of defining and evaluating the hypersingular integral. Nevertheless, the main computational task in implementing Eq. (10) is the evaluation of the singular integrals. For two dimensional problems there are a number of techniques available, *e.g.*, Hölzer (1993), Frangi and Novati (1996). In this work, the singular integration is accomplished by means of direct hybrid analytical/numerical algorithms, as described by Gray (1998) .

In regards to the singular integration, it is important to note that the modified shape functions present no difficulties, and in fact are easily incorporated in an existing quadratic

element code. The standard quadratic and modified quarter-point shape functions can be conveniently written in the general form

$$\hat{\psi}_j(t) = \psi_j(t) + \alpha \ \beta_j \ t(1-t)(1-2t) \ . \tag{11}$$

Here α is used to distinguish a crack tip element ($\alpha = 1$) from a regular element ($\alpha = 0$); the values for the constants β are $\beta_1 = \beta_3 = \pm\ 2/3$ and $\beta_2 = \mp\ 4/3$, and the upper or lower sign is employed if the crack tip is located at the first ($t = 0$) or third node ($t = 1$), respectively. In the latter case, by letting $s = 1 - t$, one again obtains the modified shape functions in Eq. (5) in terms of the variable s.

From this form it is clear that implementing the modified crack tip only requires the additional integration of the $t(1-t)(1-2t)$ expression. As this function is zero at the three nodes, it only contributes to the "lower order" singular terms, and in these terms it simply changes some polynomial coefficients. Thus, the analytical integration codes built for the standard quadratic shape functions (Gray 1998) can be re-used here with only minor modification.

4 Test Calculations

SIFs provided by the quarter-point elements (both modified and standard) will be calculated by means of the Displacement Correlation Technique (DCT). The point here is to assess the quality of the modified quarter point element by means a very simple method such as the DCT. The general expression of SIFs by means of the DCT technique are given by

$$\begin{aligned} K_I &= \frac{G}{\kappa+1} \lim_{r\to 0} \sqrt{\frac{2\pi}{r}} \ \Delta u_2 \\ K_{II} &= \frac{G}{\kappa+1} \lim_{r\to 0} \sqrt{\frac{2\pi}{r}} \ \Delta u_1 \end{aligned} \tag{12}$$

where Δu_k is the COD in the coordinate system associated with the crack tip under consideration, G is shear modulus, and ν is Poisson's ratio,

$$\kappa = 3 - 4\nu \quad \text{(plane strain)} \quad , \qquad \kappa = \frac{3-\nu}{1+\nu} \quad \text{(plane stress)} \quad . \tag{13}$$

By using the modified quarter-point (QP) shape functions in Eq. (5), one gets (the crack tip is assumed to be at the first node A, see the schematic of parameter space in Figure

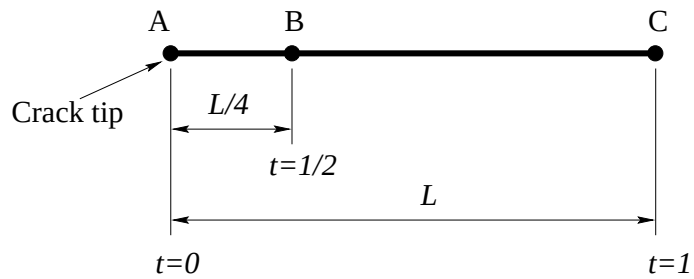

Figure 2: Crack tip element.

2)

$$\begin{aligned} \Delta u_k &= \Delta u_k^{\mathrm{B}}\ \hat{\psi}_2(t) + \Delta u_k^{\mathrm{C}}\ \hat{\psi}_3(t) \\ &= \frac{1}{3}(8\Delta u_k^{\mathrm{B}} - \Delta u_k^{\mathrm{C}})\ t + \frac{4}{3}(\Delta u_k^{\mathrm{C}} - 2\Delta u_k^{\mathrm{B}})\ t^3 \end{aligned} \tag{14}$$

Use of (14) in (12), with $t = \sqrt{r/L}$, yields

$$\begin{aligned} K_I &= \frac{G}{3(\kappa+1)}\sqrt{\frac{2\pi}{L}}\ (8\Delta u_2^{\mathrm{B}} - \Delta u_2^{\mathrm{C}}) \\ K_{II} &= \frac{G}{3(\kappa+1)}\sqrt{\frac{2\pi}{L}}\ (8\Delta u_1^{\mathrm{B}} - \Delta u_1^{\mathrm{C}}) \end{aligned} \tag{15}$$

Thus, SIFs are given directly in terms of the nodal values of the crack opening displacement at the crack tip element.

In order to assess the various features of the modified quarter-point element, the following examples are presented:

1. Single interior crack

   1.1 Mode I case

   1.2 Mixed-mode case

2. Pair of interacting collinear cracks

3. Pair of interacting circular-arc cracks

4. 'Off-center' crack

5. Three-point bending specimen

In the presentation below, the modified QP is compared with the standard quarter point element. For all examples, consistent units are used and the following material constants are employed: Young's modulus $E = 0.36$, Poisson's ratio $\nu = 0.27$. The first three examples deal with infinite body problems and the numerical results are compared with the analytical solutions given by Tada *et al.* (1973), whereas the last two examples involve finite body cases.

4.1 Single interior crack

Consider a plate containing a single interior crack which is oriented arbitrarily with respect to the angle θ, as illustrated Figure 3. The plate is subjected to the remote uniaxial tension $\sigma = 100$ applied along the y-axis. The crack length is 2a = 0.4 and the plate dimensions are 2H = 2W = 200 which can be approximated as an unbounded domain in this case. Two cases will be considered, the mode I case ($\theta = 0$), and the mixed-mode case ($0 < \theta < \pi/2$).

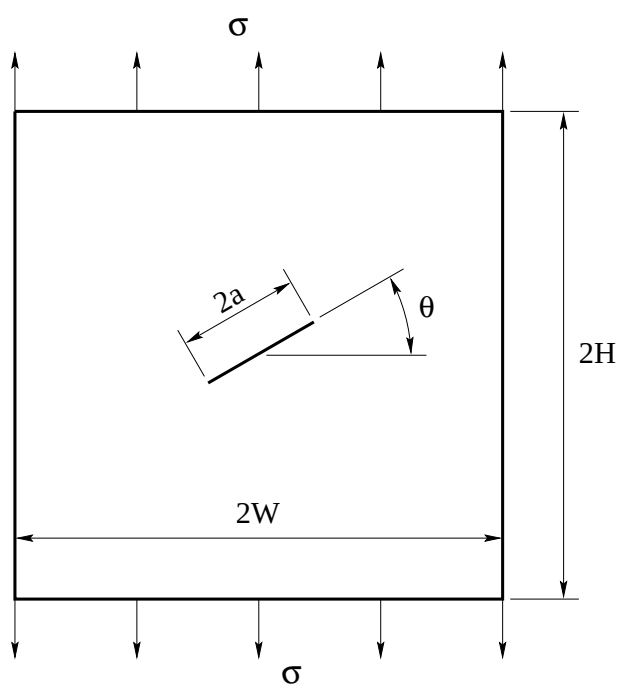

Figure 3: Single interior crack.

4.1.1 Mode I case ($\theta = 0$)

Consider a single interior crack aligned along the x-axis, *i.e.* $\theta = 0$ (see Figure 3). The crack opening displacements (displacement discontinuities along the crack) Δu_2 are depicted in Figure (4), with the crack being discretized into 10 uniform quadratic elements. It can be seen that the SG-BEM solutions using the standard and modified QP elements are in very good agreement with the analytical solution.

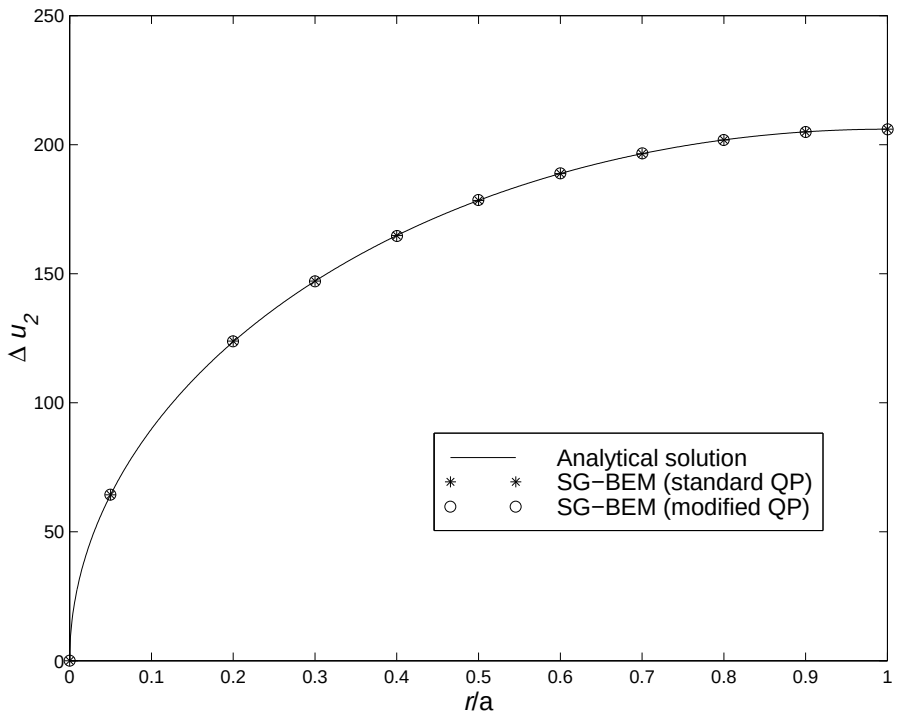

Figure 4: Crack opening displacement solutions.

With this mesh, however, while the modified QP element can give very accurate value of the mode-I SIF ($K_I/K_I^{\text{exact}} = 0.9999$), the result obtained from the standard QP element is ($K_I/K_I^{\text{exact}} = 1.0233$). A finer mesh needs to be employed in the standard QP case to improve the result while the solution obtained from the modified QP case is mostly insensitive with the mesh (see Table 1). In fact, when the modified QP shape functions are used, the solution is slightly less accurate as the mesh becomes finer. This may be explained by the fact that the crack tip element should be 'long enough' in order for the t^3 terms in the shape functions (see Eqs. (5) and (14)) to exhibit their presence. This is another advantage of the modified QP element because it means that the mesh on the crack does not need to be excessively refined in order to obtain accurate results.

Table 1: K_I/K_I^{exact} as function of the number of crack elements

# crack elements	Standard QP	Modified QP
8	1.0298	1.0002
10	1.0233	0.9999
20	1.0110	0.9996
30	1.0070	0.9996
40	1.0050	0.9995
50	1.0038	0.9995
60	1.0030	0.9995
70	1.0025	0.9995
80	1.0021	0.9995

4.1.2 Mixed-mode case ($0 < \theta < \pi/2$)

Consider mixed-mode situation where $0 < \theta < \pi/2$. Table 2 reveals that the errors of K_I and K_{II} evaluated from the standard and modified QP elements are consistent and uniform no matter what value of θ. Again, with ten crack elements employed, modified QP shape functions give excellent accuracy for both K_I and K_{II}.

Table 2: Normalized SIFs as functions of angle θ

Angle	Standard QP		Modified QP	
θ	K_I/K_I^{exact}	$K_{II}/K_{II}^{\text{exact}}$	K_I/K_I^{exact}	$K_{II}/K_{II}^{\text{exact}}$
$\pi/12$	1.0233	1.0233	0.9999	0.9999
$\pi/6$	1.0233	1.0233	0.9999	0.9999
$\pi/4$	1.0233	1.0233	0.9999	0.9999
$\pi/3$	1.0233	1.0233	0.9999	0.9999

4.2 Pair of interacting collinear cracks

This is an example of two interacting cracks which have the same length $2a = 0.2$ and are separated by a gap b (see Figure (5)). The plate can be considered as an infinite

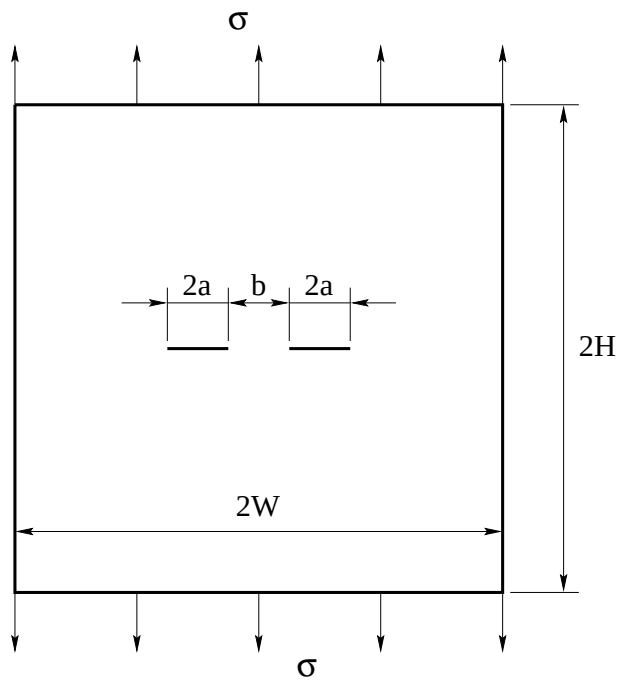

Figure 5: Pair of interacting collinear cracks.

domain by using the same dimensions as those in the previous example. The cracks are subjected to uniaxial tension $\sigma = 100$ applied in the direction perpendicular to the cracks. The mode-I SIF at the inner crack tips is of interest.

For the case $b = 4a$, the numerical results for (K_I/K_I^{exact}), as a function of the number of elements per crack, are virtually the same as for the central crack example. The same remarks as above therefore apply here. The effect of crack interaction is depicted in Figure 6 where ten elements per crack are employed. The numerical error of K_I increases as the gap between the cracks decreases. However, it can be seen that the increase in error rate for the standard QP is higher as the cracks come closer to each other. Moreover, the error from the modified QP is always much lower no matter what the value of the gap. This error is less than 1% even when the ratio b/a is less than one-quarter.

4.3 Pair of interacting circular-arc cracks

It is generally recognized that the Displacement Correlation Technique combined with the standard QP shape functions usually produce poor accuracy for SIFs in case of mixed-mode situations. Use of modified QP elements instead can improve considerably this

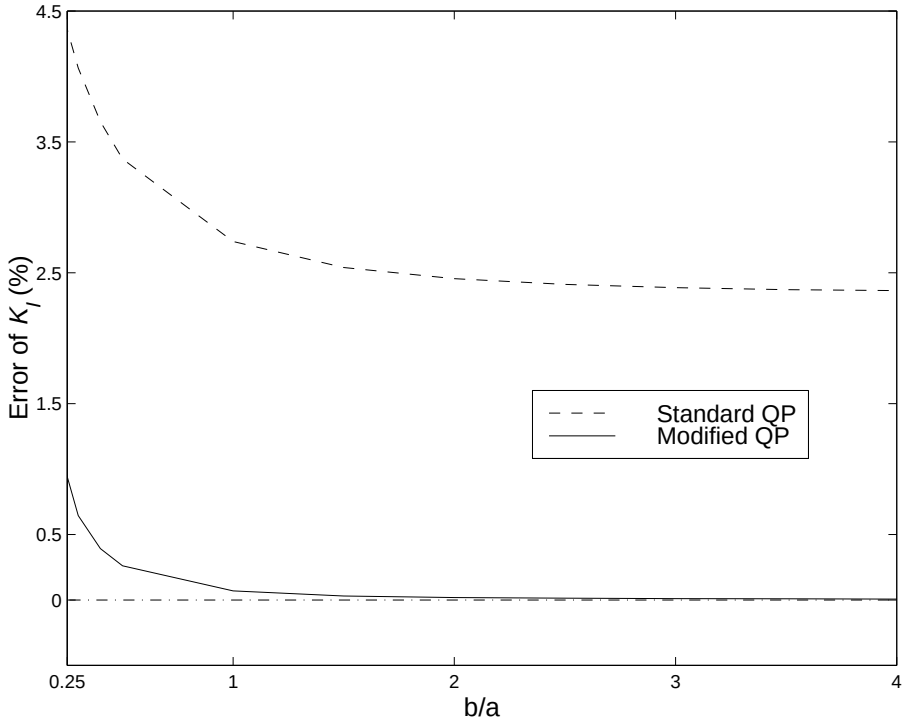

Figure 6: Effect of crack interaction.

accuracy as shown in this example.

Consider a mixed-mode example through a pair of circular-arc cracks of radius R = 0.1, angle $\theta = \pi/2$, embedded in a plate of dimension (2H $\times$ 2W), and subjected to remote biaxial tension σ as shown in Figure 7. The same plate dimension as in two previous examples is chosen again in order to consider this problem as an unbounded domain. Five elements (of uniform length) per crack are used. For comparison purposes, an asymptotic solution for the COD, valid as $r \to 0$, can be derived from the exact SIF values,

$$\Delta u_2^{\text{asy}} = \frac{\kappa+1}{G}\sqrt{\frac{r}{2\pi}}\ K_I^{\text{exact}}$$
$$\Delta u_1^{\text{asy}} = \frac{\kappa+1}{G}\sqrt{\frac{r}{2\pi}}\ K_{II}^{\text{exact}}\ . \tag{16}$$

Figure 8 illustrates the SG-BEM result versus the asymptotic solution for the crack opening displacements Δu_2 and Δu_1 along the crack tip element.

Although Δu_2 given by the standard and modified QP are seen to be in very good agreement with Δu_2^{asy} near the crack tip as shown in the left plot of Figure 8, the accuracy of the K_I obtained from the modified QP is much better as shown in Table 3. On the other

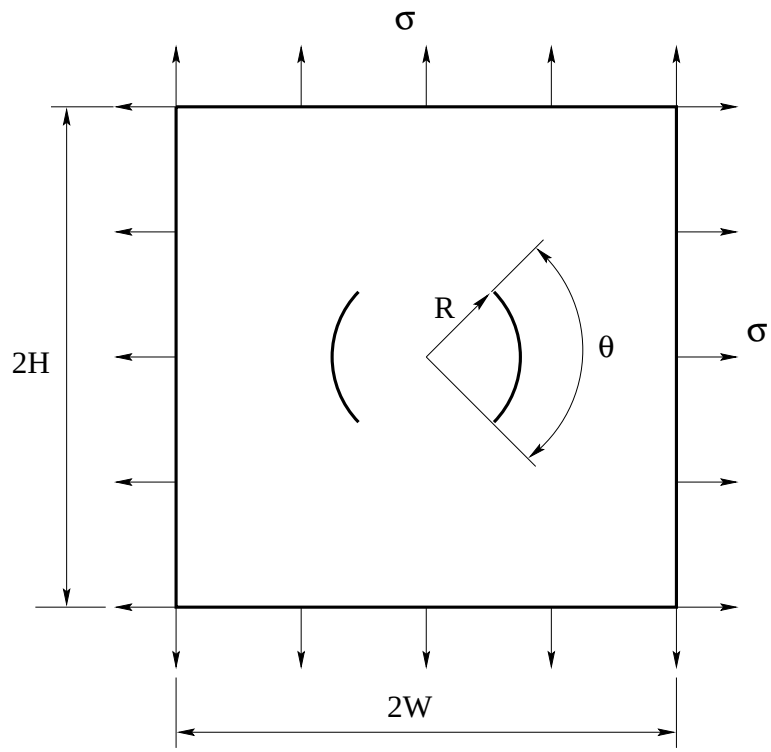

Figure 7: Pair of circular-arc cracks.

hand, while Δu_1 given by the modified QP is in good agreement with the asymptotic solution, this is not the case for Δu_1 obtained from the standard QP (see the right plot of Figure 8). This explains why the K_{II} from the modified QP is much more accurate than that from the standard one as seen in Table 3.

The effect of crack interaction on the SIFs for modes I and II (as a function of θ) is depicted in Figure 9. For mode-I SIF, similar remarks as those derived in the pair of aligned cracks can also be observed here. However, while the mode-II SIF obtained from the standard QP is mostly unchanged with the increase of θ, the modified QP element helps to dramatically improve this quantity, even where the crack tips are very close ($\theta \approx \pi$).

4.4 'Off-center' crack

This example deals with mixed-mode case in a finite body. Consider a crack whose location and orientation are arbitrary in a plate, subjected to the remote uniaxial tension σ applied

Table 3: Normalized SIFs.

Normalized SIFs	Standard QP	Modified QP
K_I/K_I^{exact}	1.0711	1.0047
$K_{II}/K_{II}^{\text{exact}}$	0.7512	0.9625

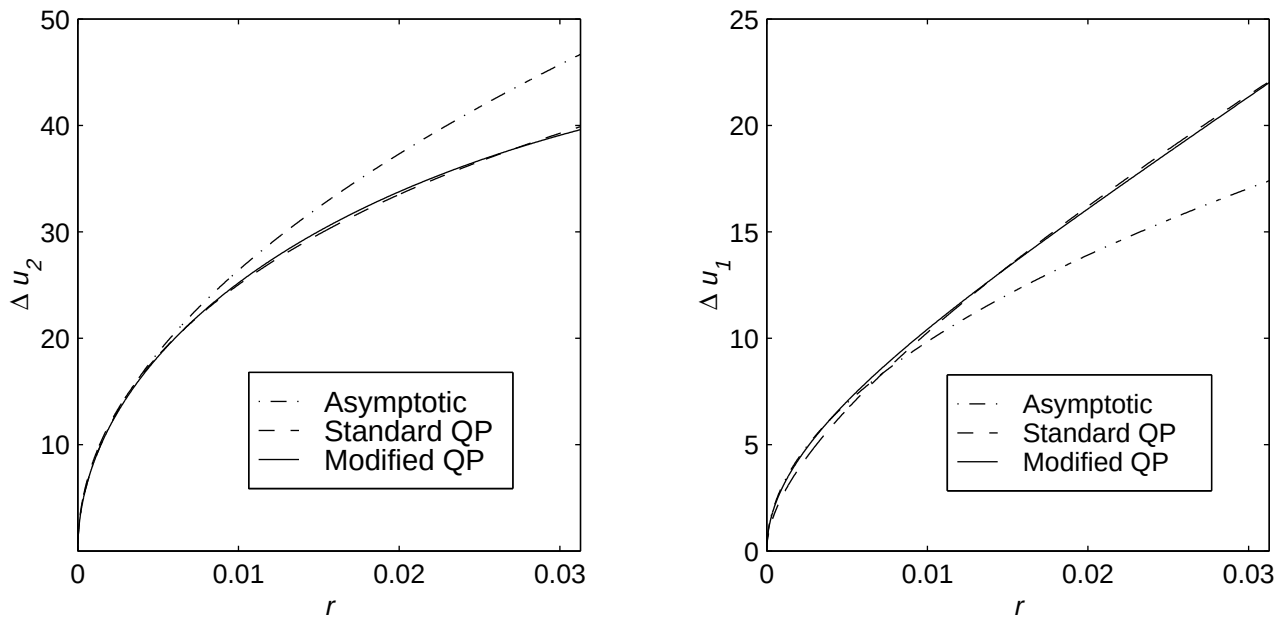

Figure 8: Solutions for the crack opening displacement $\Delta\mathbf{u}$ along the crack tip element.

along the y-axis as shown in Figure 10. The following geometry data are studied: 2W = 2H = 2, 2a = 0.5 and $e_x = e_y = 0.5$. The standard and modified QP shape functions are used with 10 uniform elements on the crack. Numerical results, normalized by $\sigma\sqrt{\pi a}$, for mode I and II SIFs at both crack tips A and B are presented in Tables 4 and 5 along with those given in Yuanhan (1991). It can be observed that all the solutions obtained from the modified QP shape functions are much closer to the reference than those from the standard ones. Note that the reference results are not the exact solution because they are also obtained by another numerical approach. However, since the approach used is the boundary collocation method which is supposed to be more accurate than the displacement correlation technique, it can be concluded once again that mixed-mode SIFs are improved by using the modified QP shape functions. Finally, these improved results

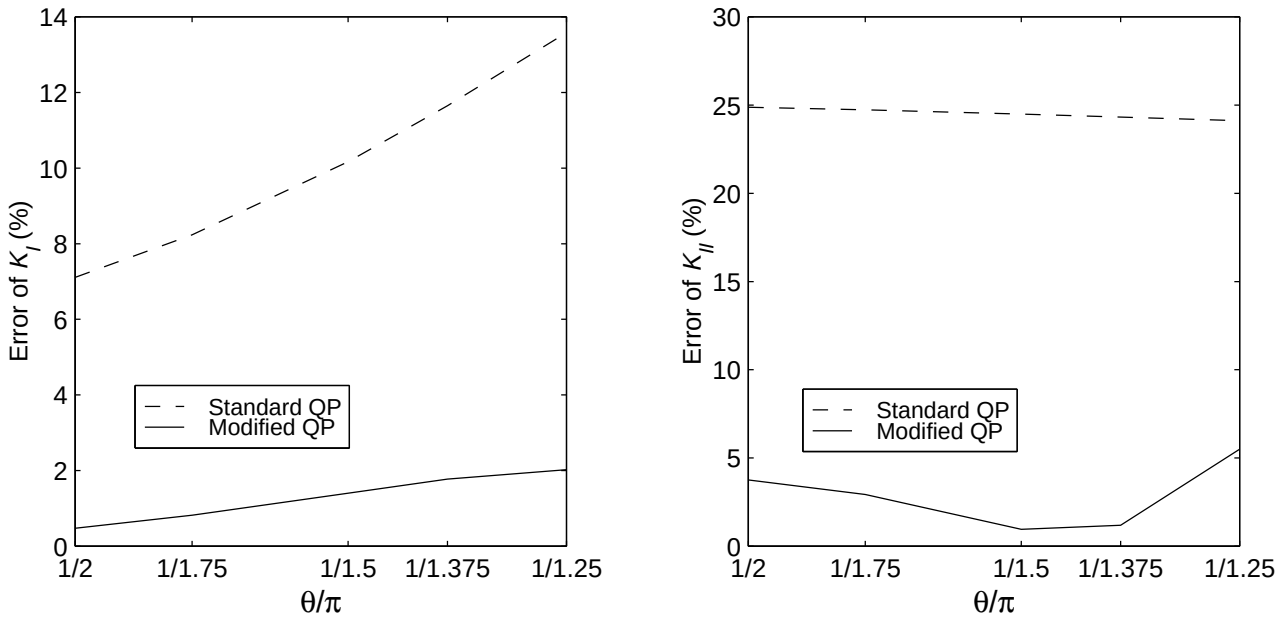

Figure 9: Effect of crack interaction on SIFs.

are illustrated in Figure 11 as functions of angle θ.

Table 4: Normalized SIFs at crack tip A as functions of crack angle θ

Angle θ	$K_I^{\mathrm{A}}/\sigma\sqrt{\pi \mathsf{a}}$			$K_{II}^{\mathrm{A}}/\sigma\sqrt{\pi \mathsf{a}}$		
	Standard QP	Modified QP	Reference	Standard QP	Modified QP	Reference
0	1.2259	1.2022	1.2001	0.0306	0.0274	0.0271
$\pi/6$	0.9096	0.8926	0.8918	0.4977	0.4869	0.4870
$\pi/3$	0.3097	0.3034	0.3030	0.4842	0.4743	0.4738
$\pi/2$	0.0000	0.0000	0.0000	0.0000	0.0000	0.0000
$2\pi/3$	0.2807	0.2767	0.2764	-0.5004	-0.4891	-0.4873
$5\pi/6$	0.8987	0.8819	0.8794	-0.5328	-0.5189	-0.5154
π	1.2540	1.2278	1.2227	-0.0469	-0.0436	-0.0426

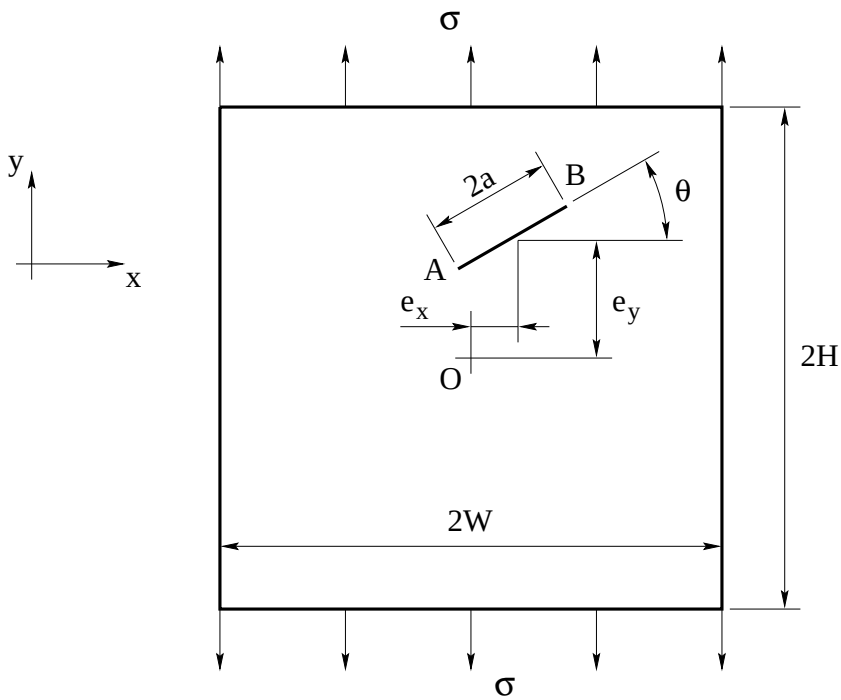

Figure 10: 'Off-center' crack.

Table 5: Normalized SIFs at crack tip B as functions of crack angle θ

Angle θ	$K_I^{\mathrm{B}}/\sigma\sqrt{\pi \mathsf{a}}$			$K_{II}^{\mathrm{B}}/\sigma\sqrt{\pi \mathsf{a}}$		
	Standard QP	Modified QP	Reference	Standard QP	Modified QP	Reference
0	1.2540	1.2278	1.2227	-0.0469	-0.0436	-0.0426
$\pi/6$	0.9665	0.9460	0.9431	0.4950	0.4844	0.4832
$\pi/3$	0.3178	0.3109	0.3086	0.5067	0.4953	0.4933
$\pi/2$	0.0000	0.0000	0.0000	0.0000	0.0000	0.0000
$2\pi/3$	0.3347	0.3254	0.3217	-0.4918	-0.4816	-0.4790
$5\pi/6$	0.9527	0.9315	0.9274	-0.4646	-0.4577	-0.4580
π	1.2259	1.2022	1.2001	0.0306	0.0274	0.0271

4.5 Three-point bending beam

The last example deals with a surface crack and bending deformation. A three-point bending beam under opening mode as shown in Figure 12 is studied. Mode-I SIF is

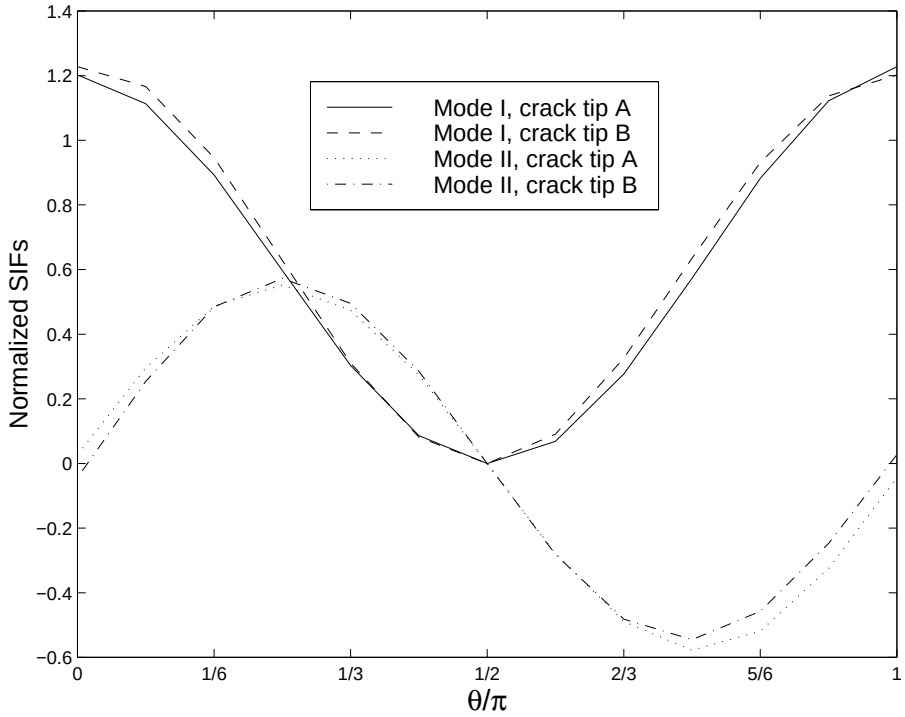

Figure 11: Normalized SIFs as functions of angle θ.

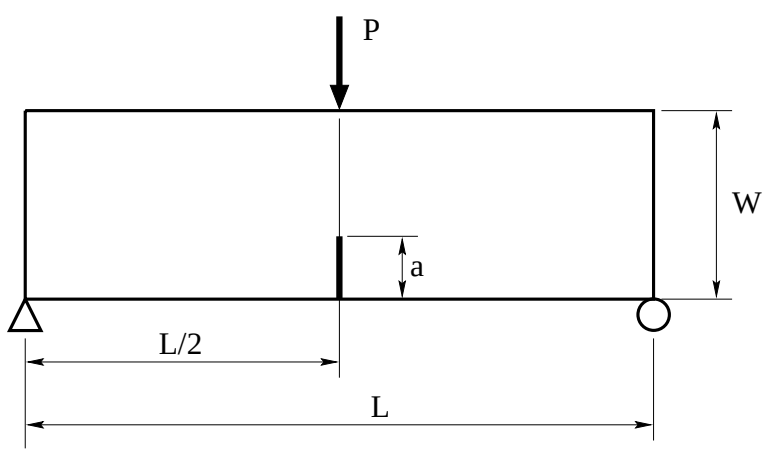

Figure 12: Three-point notched bending beam.

evaluated for a wide range of geometry of the beam and crack using crack elements of uniform length Δa = 0.02W. The SG-BEM results are compared with the analytical solution proposed by Guinea *et al.* (1998) and listed in Table 6. Deviation of the standard

and modified QP results from the reference is illustrated in Figure 13. It can be seen that all results obtained from the modified QP shape functions are in better agreement with the reference except in case L/W = 2.5 and a/W = 0.1. Since the Guinea et al.'s solution is a good but not an absolutely exact reference, this incompatibility might serve as an indication to revise the proposed expression in the above case.

Table 6: K_I/K_I^{ref} as functions of L/W and a/W

a/W	L/W = 2.5		L/W = 8	
	Standard QP	Modified QP	Standard QP	Modified QP
0.1	0.9898	0.9870	1.0020	0.9981
0.2	0.9816	0.9855	0.9959	0.9995
0.3	0.9800	0.9868	0.9941	1.0011
0.4	0.9797	0.9887	0.9914	1.0011
0.5	0.9791	0.9905	0.9868	0.9990
0.6	0.9770	0.9916	0.9791	0.9946
0.7	0.9722	0.9920	0.9657	0.9862
0.8	0.9610	0.9908	0.9546	0.9851

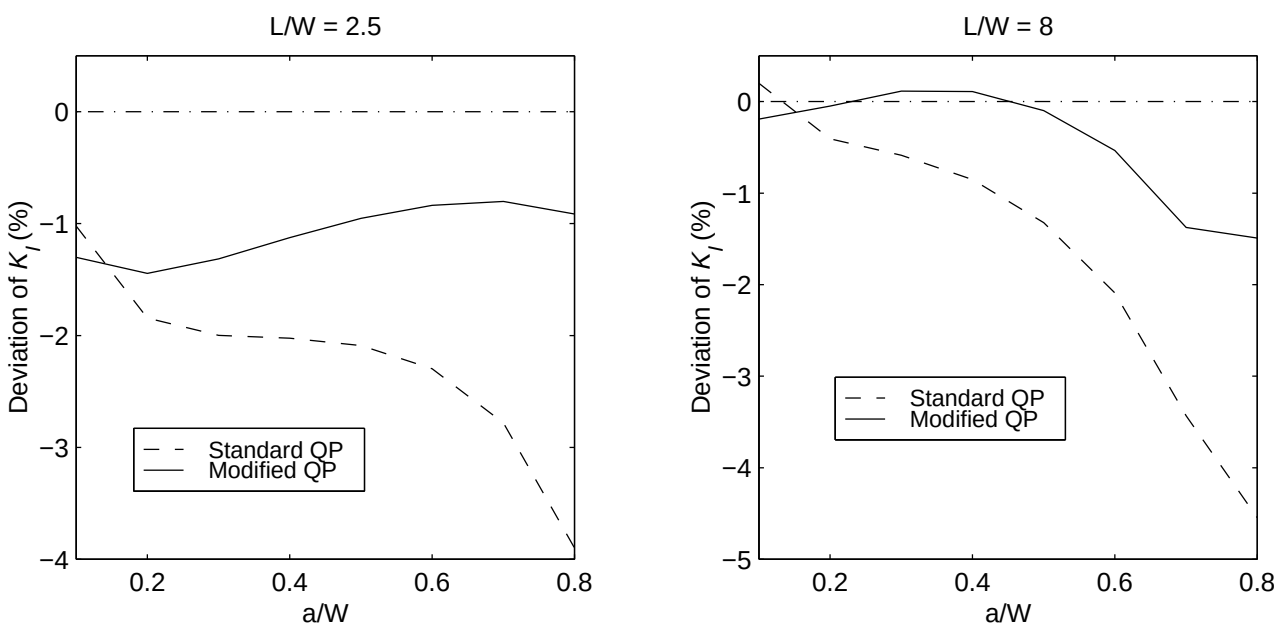

Figure 13: Deviation of the standard and modified QP results from the reference.

5 Conclusions

The modified quarter-point crack tip element defined in this paper has been shown to produce highly accurate SIFs. This is the case even though the calculations employed relatively coarse meshes, combined with the very simple *local* method (displacement correlation) to calculate SIFs. Moreover, the modified quarter-point element has been shown to be consistently superior to the standard quarter-point element. Thus, this improved element should be very useful for crack propagation simulations, as in these calculations is difficult to minutely control the meshing.

As the modified element only serves to improve the local COD solution at the tip, it is not expected to have a significant impact on non-local SIF evaluation methods, *e.g.*, J-integral. However, the hope is that combining this element with simple and computationally inexpensive local SIF methods will produce sufficient accuracy, in both two and three dimensions.

The extension of this work to three dimensions should be possible. The first step would be to establish that the linear term constraint remains valid; extending the two-dimensional analysis in [10] appears to be straightforward. The second step, developing a modified crack tip element (again from quadratic to cubic), should follow along the same lines as presented herein. These investigations are currently being pursued by the authors.

Acknowledgments

This research was supported in part by the Applied Mathematical Sciences Research Program of the Office of Mathematical, Information, and Computational Sciences, U.S. Department of Energy under contract DE-AC05-00OR22725 with UT-Battelle, LLC. Additional support was provided by the Laboratory Directed Research and Development Program of the Oak Ridge National Laboratory. G. H. Paulino acknowledges the support from the National Science Foundation under grant CMS-9713008 (Mechanics and Materials Program).

References

[1] L. Banks-Sills, *Application of the finite element method to linear elastic fracture mechanics*, Appl. Mech. Rev., 44 (1991), pp. 447–461.

[2] R. S. Barsoum, *On the use of isoparametric finite elements in linear fracture mechanics*, Int. J. Numer. Meth. Engrg., 10 (1976), pp. 25–37.

[3] G. E. Blandford, A. R. Ingraffea, and J. A. Liggett, *Two-dimensional stress intensity factor computations using the boundary element method*, Int. J. Num. Meth. Engng, 17 (1981), pp. 387–404.

[4] M. Bonnet, *Boundary Integral Equation Methods for Solids and Fluids*, Wiley and Sons, England, 1995.

[5] M. Bonnet, G. Maier, and C. Polizzotto, *Symmetric Galerkin boundary element method*, ASME Appl. Mech. Rev., 51 (1998), pp. 669–704.

[6] C. A. Brebbia, J. C. F. Telles, and L. C. Wrobel, *Boundary Element Techniques*, Springer-Verlag, Berlin and New York, 1984.

[7] T. A. Cruse, *Boundary Element Analysis in Computational Fracture Mechanics*, Kluwer Academic Publishers, Boston, 1988.

[8] A. Frangi and G. Novati, *Symmetric BE method in two-dimensional elasticity: evaluation of double integrals for curved elements*, Computational Mechanics, 19 (1996), pp. 58–68.

[9] L. J. Gray, *Evaluation of singular and hypersingular Galerkin boundary integrals: direct limits and symbolic computation*, in Singular Integrals in the Boundary Element Method, V. Sladek and J. Sladek, eds., Advances in Boundary Elements, Computational Mechanics Publishers, 1998, ch. 2, pp. 33–84.

[10] L. J. Gray and G. H. Paulino, *Crack tip interpolation, revisited*, SIAM J. Applied Mathematics, 58 (1998), pp. 428–455.

[11] G. Guinea, J. Pastor, J. Planas, and M. Elices, *Stress intensity factor, compliance and cmod for a general three-point-bend beam*, Int. J. Fracture, 89 (1998), pp. 103–116.

[12] R. D. Henshell and K. G. Shaw, *Crack tip finite elements are unnecessary*, Int. J. Numer. Meth. Engrg., 9 (1975), pp. 495–507.

[13] S. M. Hölzer, *How to ideal with hypersingular integrals in the symmetric BEM*, Comm. Num. Meth. Engng., 9 (1993), pp. 219–232.

[14] Á. Horváth, *Higher-order singular isoparametric elements for crack problems*, Comm. Num. Meth. Engng., 10 (1994), pp. 73–80.

[15] I. L. Lim, I. W. Johnston, and S. K. Choi, *Application of singular quadratic distorted isoparametric elements in linear fracture mechanics*, Int. J. Numer. Meth. Engrg., 36 (1993), pp. 2473–2499.

[16] A. M. Linkov and S. G. Mogilevskaya, *Complex hypersingular integrals and integral equations in plane elasticity*, Acta Mechanica, 105 (1994), pp. 189–205.

[17] P. A. Martin, *End-point behavior of solutions to hypersingular equations*, Proc. R. Soc. Lond., A, 432 (1991), pp. 301–320.

[18] J. R. Rice, *Mathematical analysis in the mechanics of fracture*, in Fracture – An Advanced Treatise, H. Liebowitz, ed., vol. II, Pergamon Press, Oxford, 1968, pp. 191–311.

[19] F. J. Rizzo, *An integral equation approach to boundary value problems of classical elastostatics*, Quart. Appl. Math., 25 (1967), pp. 83–95.

[20] S. Sirtori, G. Maier, G. Novati, and S. Miccoli, *A Galerkin symmetric boundary element method in elasticity: formulation and implementation*, Int. J. Numer. Meth. Engrg., 35 (1992), pp. 255–282.

[21] J. Sladek and V. Sladek, *Dynamic stress intensity factors studied by boundary integro-differential equations*, Int. J. Numer. Meth. Engrg., 23 (1986), pp. 919–928.

[22] H. Tada, P. Paris, and G. Irwin, *The Stress Analysis of Cracks Handbook*, Del Research Corporation, Hellertown, Pennsylvania, 1973.

[23] M. L. Williams, *Stress singularities resulting from various boundary conditions in angular corners of plates in extension*, ASME J. Appl. Mech., 19 (1952), pp. 526–528.

[24] ——, *On the stress distribution at the base of a stationary crack*, ASME J. Appl. Mech., 24 (1957), pp. 109–114.

[25] W. Yuanhan, *Asymmetric crack problems calculated by the boundary collocation method*, Engineering Fracture Mechanics, 40 (1991), pp. 133–143.

Appendix

For convenience, the kernel functions for the displacement and stress boundary integral equations are provided below. The Kelvin solution U_{kj} is well known to be

$$U_{kj}(P,Q) = \frac{1}{8\pi G(1-\nu)}\left[-(3-4\nu)\delta_{kj}\log(r) + r_{,k}r_{,j}\right] \ . \tag{17}$$

Differentiating this displacement to obtain traction results in

$$\begin{aligned} T_{kj}(P,Q) \ &= \ -\frac{1}{4\pi(1-\nu)r}\left[\left\{(1-2\nu)\delta_{kj} + 2r_{,k}r_{,j}\right\}\frac{\partial r}{\partial n} - \right. \\ &\qquad \left. (1-2\nu)\left\{n_j r_{,k} - n_k r_{,j}\right\}\right] \ . \end{aligned} \tag{18}$$

The kernels $D_{lkm}(P,Q)$ (singular) and $S_{lkm}(P,Q)$ (hypersingular) for the stress equation are given by (see Brebbia *et al.* 1984, Eqs. (5.69) and (5.70))

$$\begin{aligned} D_{lkm} \ &= \ \frac{1}{4\pi(1-\nu)r}\left[(1-2\nu)\left\{\delta_{lm}r_{,k} + \delta_{km}r_{,l} - \delta_{lk}r_{,m}\right\} + 2r_{,l}r_{,k}r_{,m}\right] \\ S_{lkm} \ &= \ \frac{\mu}{2\pi(1-\nu)r^2}\left[2\frac{\partial r}{\partial \mathbf{n}}\left(\left\{1-2\nu\right\}\delta_{lk}r_{,m} + \nu\left(\delta_{km}r_{,l} + \delta_{lm}r_{,k}\right) - 4r_{,l}r_{,k}r_{,m}\right)\right. \\ &\qquad +(1-2\nu)\left(2n_m r_{,l}r_{,k} + n_k\delta_{lm} + n_l\delta_{km}\right) \\ &\qquad\quad \left. +2\nu\left(n_l r_{,k}r_{,m} + n_k r_{,l}r_{,m}\right) - (1-4\nu)n_m\delta_{lk}\right] \ . \end{aligned} \tag{19}$$

In these equations, ν is Poisson's ratio, μ is shear modulus, δ_{ij} is the Kronecker delta, $r_{,i} = \partial r/\partial q_i$, and q_i is the ith coordinate of the field point Q.